Available online at www.sciencedirect.com

ScienceDirect

Publishing Services by Elsevier

International Journal of Naval Architecture and Ocean Engineering 9 (2017) 404–417

http://www.journals.elsevier.com/international-journal-of-naval-architecture-and-ocean-engineering/

Numerical analysis of dynamic response of jacket structures subject to slamming forces by breaking waves

Chanjo Woo [a], Insik Chun [b,*], Christy Ushanth Navaratnam [c], Jaeseol Shim [d]

[a] *Mapes Engineering Co. Ltd., Seoul, South Korea*

[b] *Department of Infra System Engineering, Konkuk University, Seoul, South Korea*

[c] *Department of Hydraulic and Environmental Engineering, Norwegian University of Science and Technology, Trondheim, Norway*

[d] *Korea Institute of Ocean Science and Technology, Seoul, South Korea*

Received 28 August 2016; revised 11 November 2016; accepted 19 November 2016

Available online 13 January 2017

Abstract

The present study numerically analyzed the dynamic behavior of 3D framed structures subject to impulsive slamming forces by violent breaking waves. The structures were modeled using multiple lumped masses for the vertical projections of each member, and the slamming forces from the breaking waves were concentrated on these lumped masses. A numerical algorithm was developed to properly incorporate the slamming forces into a dynamic analysis to numerically determine the structural responses. Then, the validity of the numerical analysis was verified using the results of an existing hydraulic experiment. The numerical and experimental results for various model structures were generally in good agreement. The uncertainties concerning the properties of the breaking waves used in the verification are also discussed here.

Keywords: Breaking wave; Slamming force; Dynamic analysis; Lumped mass method; Framed jacket structures

1. Introduction

Most offshore structures are installed in relatively deep sea areas, where incoming waves are normally symmetrical about the wave crest, as shown in Fig. 1(a). The design forces are determined by applying the well-known Morison formula for water particle kinematics (velocity and acceleration), which are normally provided by a nonlinear wave theory. However, there have also been many cases where structures have been placed in shallow sea areas. Recently, wind turbine towers have often been constructed in shallow coastal zones. Moreover, marine observation towers are constructed in shallow underwater shoals in order to reduce their construction costs. In these cases, incoming waves may be incident to the structures in the form of plunging breaking waves, as shown in Fig. 1(b). An impulsive slamming force occurs when the downstream skewed surface of a breaking wave abruptly impinges on the members comprising an offshore structure. The mechanism of this slamming force is thus completely different from that of the non-breaking symmetrical wave force dictated by the Morison formula, generally producing much higher forces. Hence the slamming force can cause not only a severe damage on sub-structures but also a violent vibration of the whole structure which may impose secondary damages on deck components or equipments even before the waves directly hit the deck.

The research on the slamming force produced by breaking waves has a fairly long history, but most of it has been experimental. Initially, studies were conducted on the impact force generated when a body suddenly contacts the water surface (von Karman, 1929; Wagner, 1932; Campbell and Weynberg, 1980; Greenhow and Li, 1987). The researchers tried to find the most appropriate value for the slamming coefficient in the range of π to 2π, which could be substituted

* Corresponding author.
E-mail address: ischun@konkuk.ac.kr (I. Chun).
Peer review under responsibility of Society of Naval Architects of Korea.

http://dx.doi.org/10.1016/j.ijnaoe.2016.11.005

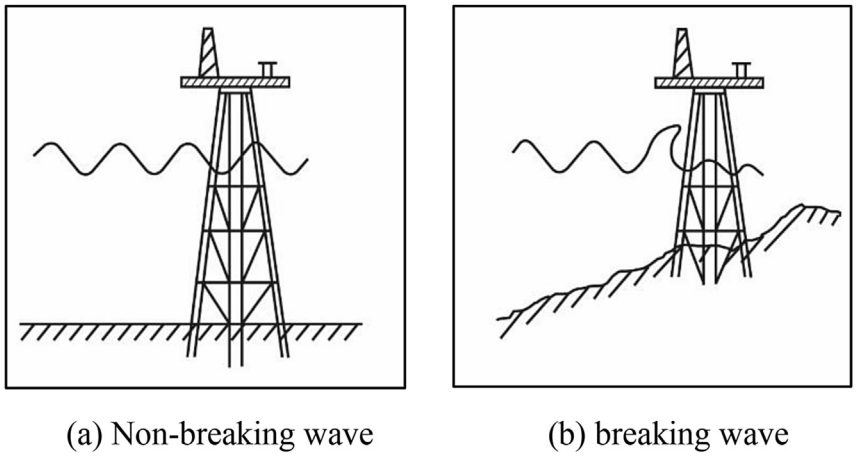

Fig. 1. Incident wave conditions to offshore structure.

for the drag coefficient in the well-known drag force formula. Later, Hall (1958) and Ross (1959) proposed experimental formulas for the slamming force on a vertical cylinder with a circular cross-section. Many researchers, including Goda et al. (1966), Honda and Mitsuyasu (1974), Wiegel (1982), Kjeldsen et al. (1986), and Apelt and Piorewicz (1987) dealt with the slamming force acting on a single vertical pile. Dalton and Nash (1976), and Sarpkaya (1978), considered the slamming force on a horizontal pile. On the other hand, Tanimoto et al. (1986), and recently Wienke and Oumeraci (2005), included inclined slender piles in their experimental studies. A few studies, including those by Goda et al. (1966), Tanimoto et al. (1986), and Wienke and Oumeraci (2005), proposed semi-empirical formulas for predicting the slamming forces acting on a single vertical pile based on experimental results. However, none of these researchers were concerned with the numerical determination of slamming forces on more realistic 3D framed structures. Recently, a research group at the Norwegian University of Science and Technology (Aashamar, 2012; Chella et al., 2012; Navaratnam, 2013) conducted the first study on the slamming forces on various framed structures. However, their studies were also mainly experimental.

Some studies, including Choi et al. (2015), applied Computational Fluid Dynamics (CFD) based on Navier–Stokes equations to calculate the slamming forces acting on single vertical piles. At present, however, a CFD method does not appear to be very promising in real structural design practices because of its long calculation time or inadequate computer capacity. Recently, Chun et al. (2016) proposed a simple numerical algorithm for calculating the slamming forces acting on 3D framed structures. The framed structures were first modeled using multiple lumped masses for the vertical projections of each member, and the slamming forces produced by breaking wave were concentrated on these lumped masses. This made it possible to avoid the inherent difficulty of applying slamming forces to structural members with various orientations in 3D framed structures.

The present paper presents more details on a numerical analysis incorporating the slamming forces into an existing routine for the dynamic analyses of framed structures. Then, the performance of this numerical analysis method is verified using the experimental results by Navaratnam (2013), followed by a discussion of the uncertainties of the breaking waves used in the experiment. Finally, a recommended procedure for the application of the present numerical analysis method to the design of prototype structures is also proposed.

2. Dynamic analysis of jacket structures by slamming force

2.1. Lumped mass method

A dynamic analysis is performed here using a lumped mass method, where the masses of the members comprising the structure are represented by equivalent lumped masses placed on the joints connecting the members, as shown in Fig. 2. The lumped area A_p and volume B_p at a joint can be determined by summing halves of the vertically projected areas and volumes of all the members connected to the joint. The lumped mass $\widehat{M}_p$ can be determined for the whole length of the members, while taking into account the buoyancy force of submerged members and water mass captured inside the members. The details are well described in Dawson (1983).

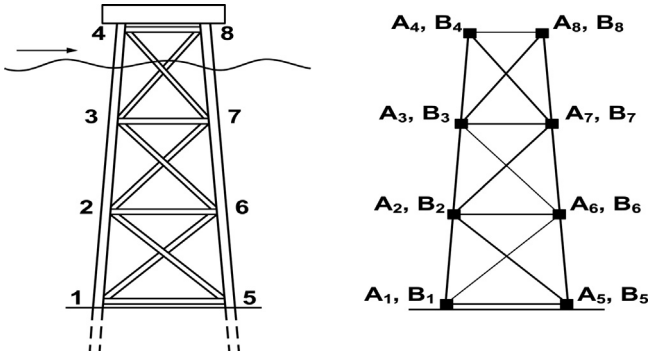

Fig. 2. Lumped areas and volumes (reproduced from Dawson (1983)).

Although each lumped mass could be separately considered in the dynamic analysis, several horizontal layers representing the dynamic behaviors of the lumped masses on each layer are here employed as in Dawson (1983). That is, the structure in Fig. 3 is represented by four layers (1–5, 2–6, 3–7, and 4–8). Suppose that the whole structure is modeled with N_L layers. Then, the wave force F_i^w acting on the i-th layer composed of N_i joints can be determined using the j-th lumped area A_{ij} and lumped volume B_{ij} as follows:

$$F_i^{\omega} = \sum_{j=1}^{N_i}\left[\frac{1}{2}\rho C_D A_{ij}\left|u'_{ij}\right|u'_{ij} + \rho C_I B_{ij} a_{ij} - \rho(C_I-1)B_{ij}\ddot{U}_{ij}\right] \quad (1)$$

where C_D = drag coefficient, C_I = inertia coefficient, U_{ij} = horizontal joint displacement, $\dot{U}_{ij}$ = horizontal joint velocity, $\ddot{U}_{ij}$ = horizontal joint acceleration, u_{ij} = horizontal water particle velocity, a_{ij} = horizontal water particle acceleration, and $u'_{ij} = u_{ij} - \dot{U}_{ij}$. The values of u_{ij} and a_{ij} can be calculated using a wave theory.

Assuming that the dynamic behaviors of all the joints on each layer are identical, as follows:

$$U_{ij} = U_i;\ j = 1,\ldots,N_i \quad (2)$$

we can rewrite Eq. (1) as

$$F_i^{\omega} = F_i^{*} - \rho(C_I-1)B_i\ddot{U}_i \quad (3)$$

where

$$F_i^{*} = \sum_{j=1}^{N_i}\left[\frac{1}{2}\rho C_D A_{ij}\left|u'_{ij}\right|u'_{ij} + \rho C_I B_{ij} a_{ij}\right] \quad (4)$$

$$B_i = \sum_{j=1}^{N_i} B_{ij} \quad (5)$$

The dynamic motion of the layers produces inertia and damping forces as follows:

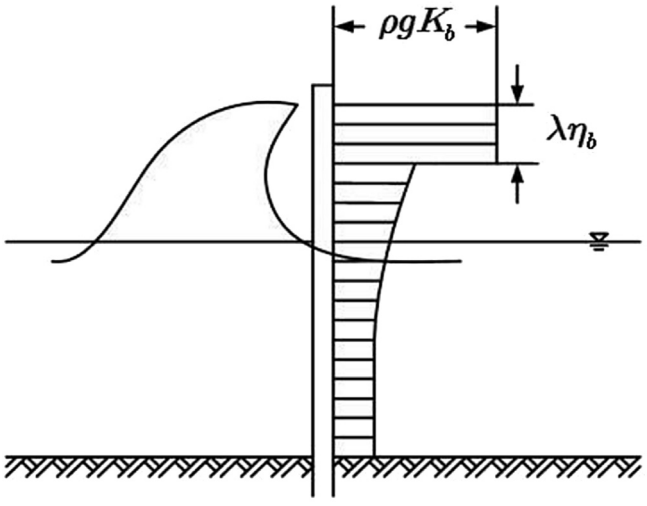

Fig. 3. Occurrence of slamming force by breaking wave.

$$F_i^{I} = \sum_{j=1}^{N_i}\widehat{M}_{i,j}\ddot{U}_{i,j} = \widehat{M}_i\ddot{U}_i \quad (6)$$

$$F_i^{D} = \sum_{j=1}^{N_i}\widehat{C}_{i,j}\dot{U}_{i,j} = \widehat{C}_i\dot{U}_i \quad (7)$$

where $\widehat{M}_i$ = sum of lumped masses on $i-$ th layer, and $\widehat{C}_i$ = constant damping coefficient. Eq. (7) only delineates structural damping with hydrodynamic damping neglected. On the other hand, a restoring force reflecting the mutual constraint of the i-th layer and other layers can be given as

$$F_i^{R} = \widehat{K}_i\, U_i \quad (8)$$

The total force acting on the layer can thus be determined by summing up the forces in Eqs. (3), (6)–(8) as follows:

$$F_i^{T} = F_i^{*} - \rho(C_I-1)B_i\ddot{U}_i - \widehat{M}_i\ddot{U}_i - \widehat{C}_i\dot{U}_i - \widehat{K}_iU_i = 0 \quad (9)$$

Finally, we can set up the dynamic equation of the layers as follows:

$$\left[M^{*}\right]\left\{\ddot{U}_L\right\} + [C]\left\{\dot{U}_L\right\} + [K]\{U_L\} = \left\{F^{*}\right\} \quad (10)$$

where [M*], [C], and [K] denote the mass matrix, damping coefficient matrix, and stiffness matrix, respectively. The diagonal components of the mass matrix are expressed as follows:

$$M_{ii}^{*} = \widehat{M}_i + \rho(C_I-1)B_i,\ i = 1,\ldots,N_L \quad (11)$$

The following method is used for determining the stiffness matrix [K].

- Impose a load $1/N_i$ on all the joints of the i-th layer having N_i joints and then calculate the average horizontal displacement of all the joints on the j-th layer U_{ij} (i, j = 1,…, N_L) through a static analysis.
- U_{ij} constitutes the i-th row vector of a matrix $[U_L]_{N_L\times N_L}$.Then, the stiffness matrix can be determined as follows:

$$[K] = [U_L]^{-1} \quad (12)$$

The damping coefficient matrix [C] depends on the structural shape and material, and is very difficult to quantitatively determine. Generally, it is given as the Rayleigh damping, which delineates the damping coefficient as a linear combination of [M*] and [K] (Wilson, 2002). In the present study, the damping coefficient matrix is set as follows (Brebbia and Walker, 1979; Dawson, 1983, pp. 294–300):

$$[C] = 2\zeta\left[M^{*}\right] \quad (13)$$

Here, ζ denotes the damping factor given by

$$\zeta = (0.05 - 0.1)\omega_1 \quad (14)$$

where ω_1 is the 1st fundamental radian frequency. Dawson (1983) also presented a method for determining the value of

ω_1. The dynamic equation (Eq. (10)) for a non-damped periodic motion is

$$\left[M^*\right]\left\{\ddot{U}_L\right\} + [K]\{U_L\} = 0 \tag{15}$$

Assuming that the displacement $\{U_L\}$ has a radian frequency ω as follows:

$$\{U_L\} = \{U_0\}\sin \omega t \tag{16}$$

and substituting Eq. (16) into Eq. (15), we have

$$-\omega^2\left[M^*\right]\{U_0\} + [K]\{U_0\} = 0 \tag{17}$$

For Eq. (17) to have a solution, the determinant of the matrix composed of the coefficients of $\{U_o\}$ should be zero. Putting $\lambda = \omega^2$, we have a polynomial on the order of N_L. The first of the N_L roots of the polynomial is taken to be ω_1, which is used in Eqs. (14) and (13) to give $[C]$.

Eq. (10) is solved for the displacement vector $\{U_L\}$ of each layer. In the present study, Wilson-θ method (Bathe, 1982) was used to produce the time series of $\{U_L\}$. Once $\{U_L\}$ is determined, the virtual forces acting on each layer can be determined as follows:

$$\{F_L\} = [K]\{U_L\} \tag{18}$$

The calculation of the member stresses is performed as follows. When a $1/N_i$ force is placed on all the joints in the i-th layer, a static analysis using the system stiffness matrix gives the i-th column vector of the 6-DOF displacement matrix $[\overline{U}]$ for all of the joints in the structure. Then, the displacement $\{U\}$ of the joints for the layer force vector $\{F_L\}$ can be determined as follows:

$$\{U\} = \left[\overline{U}\right]\{F_L\} \tag{19}$$

Combining Eq. (18) and Eq. (19) gives

$$\{U\} = \left[\overline{U}\right][K]\{U_L\} \tag{20}$$

The member stresses can easily be obtained once the displacements of all the joints $\{U\}$ are determined.

2.2. Incorporation of slamming force into the dynamic analysis

Goda et al. (1966) postulated the occurrence of a slamming force when a breaking wave acts on a vertical pile with a diameter of D, as shown in Fig. 3. The slamming force by the breaking wave acts only in the range of $\lambda\eta_b$ below the wave crest, and a normal wave force based on Morison's formula acts below this range, where η_b is the wave crest height. λ is called the curling factor and has a value of 0.3–0.48.

In the range of the slamming force, the slamming pressure on a vertical circular pile with a diameter D is

$$f_b = \rho g K_b\left(1 - \frac{t'}{\tau_b}\right) \tag{21}$$

where

$$K_b = \frac{C_s C_b^2}{2g} \tag{22}$$

$$\mathrm{C}_b = \sqrt{2gH_b} \tag{23}$$

$$\tau_b = \frac{D}{2C_b} \tag{24}$$

Here, H_b = breaking wave height, t' = time elapsed after the first contact of the breaking wave with the pile, g = gravitational acceleration, and C_s = slamming coefficient. The slamming pressure of Eq. (21) acts only within the time duration $0 \le t' \le \tau_b$, after which the normal wave force corresponding to Morison's formula is restored. As for the slamming coefficient, numerous studies have been conducted, mainly to try to determine whether π in the Karman type or 2π in the Wagner type is correct. Goda et al. (1966) proposed the use of π based on a series of hydraulic experiments.

In the present study, it is assumed that the horizontal slamming force on each member of a framed structure can be replaced by an equivalent slamming force acting on the lumped areas defined in Fig. 2. By this, the vertical slamming forces acting on horizontal and sloping members are not taken into account. But the assumption may be quite valid from a point of overall structural stability since the major slamming force may occur horizontally in the initial progressive breaking waves. The case where the horizontal slamming force occurs around the i-th joint is schematically represented in Fig. 4. The equivalent slamming force for each case can be found using a force–moment calculation with the $i-1$ th and $i+1$ th joints, as listed in Table 1. In this table, D_i is a representative diameter, which can be calculated by dividing the lumped area of the i-th joint by the total length contributing to the lumped area. $f_{b,i}$ is the slamming pressure at the i-th joint, as shown in Fig. 3. For the dynamic analysis with the slamming force, force F_i^* in Eq. (4) is replaced by $F_{b,i}$ in Table 1 for the range of $\lambda\eta_b$.

3. Verification of dynamic analysis of slamming force

Hydraulic experiments on the dynamic displacements and stresses produced by slamming forces are very rare. No field observation with a real prototype structure has been performed anywhere in the world. Recently, the Norwegian University of Science and Technology performed a series of hydraulic experiments on the slamming forces exerted on monopiles and framed structures (Aashamar, 2012; Chella et al., 2012; Navaratnam, 2013). In the present study, the experimental results of Navaratnam (2013) were used to verify the numerical algorithm developed in the previous section.

3.1. Experimental conditions

Navaratnam (2013) measured the dynamic responses of two vertical piles and two framed structures. The framed structures were basically the same, differing only in their orientations with respect to the wave direction; one was transversely placed

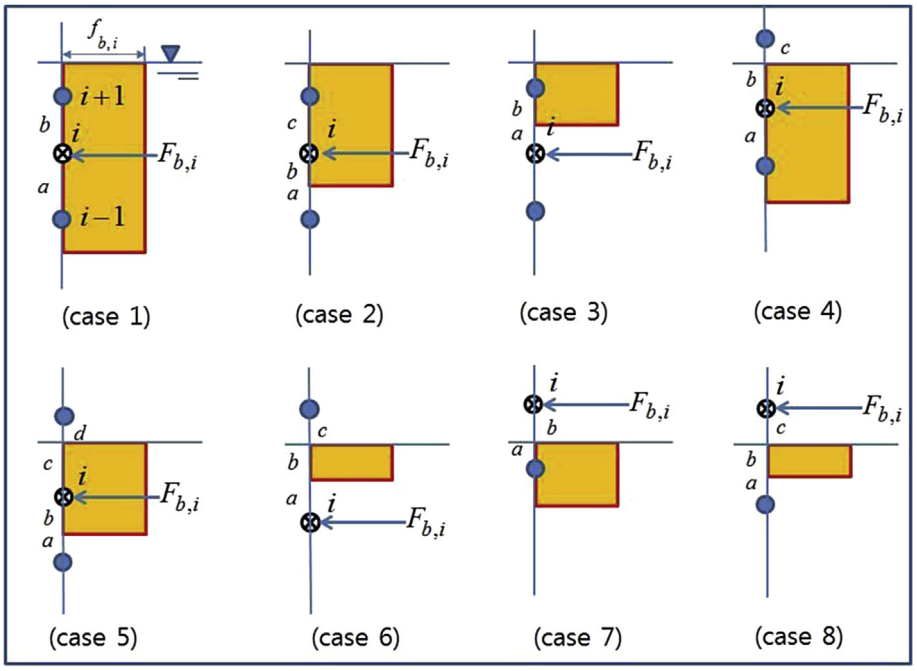

Fig. 4. Aspects of equivalent slamming force.

Table 1
Determination of equivalent slamming forces for the schemes of Fig. 4.

Cases	$F_{b,i}$
1	$0.5(a+b)f_{b,i}D_i$
2	$[b(a+0.5b)/(a+b)+0.5c]f_{b,i}D_i$
3	$[0.5b^2/(a+b)]f_{b,i}D_i$
4	$[0.5a+b(0.5b+c)/(b+c)]f_{b,i}D_i$
5	$[b(a+0.5b)/(a+b)+c(0.5c+d)/(c+d)]f_{b,i}D_i$
6	$[b(0.5b+c)/(a+b+c)]f_{b,i}D_i$
7	$[0.5a^2/(a+b)]f_{b,i}D_i$
8	$[b(a+0.5b)/(a+b+c)]f_{b,i}D_i$

(designated as "Front") and the other was longitudinally placed (designated as "Side"). The dynamic response was measured using load cells attached to the upper and lower ends of each structure. The experimental conditions are listed in Table 2. The natural frequencies of the structures (ω_1 in Eq. (17)) were calculated and presented in the table as well. The flume used in the experiment is shown in Fig. 5. Experimental waves were propagated along the 11.2-m-long flat bottom, with consecutive inclines with slopes of 1:10 and 1:20. Breaking waves were produced just downstream of the inflection point of the inclined bottoms. The experimental wave conditions were varied by controlling the period and stroke of a wave paddle.

The experimental structures and locations of the load cells used to measure the dynamic response are shown in Fig. 6. The structures were placed inside the wave flume, as shown in Fig. 7.

The measured results included the maximum total reaction forces measured by the load cells, breaking wave heights H_b, and wave crest heights η_b. The sampling interval of force measurements was 19,200 Hz. The slamming forces were deduced from the measured reaction forces. When a slamming force impinged on the experimental structures, vibrations occurred with the natural frequency of the structure, which

Table 2
Experimental conditions.

Items	Case-1	Case-2	Case-3	Case-4
Model structure	Vertical pile	Vertical pile	Front frame	Side frame
Member diameter (mm)	60	16	Vertical 16, sloping 12	Vertical 16, sloping 12
Member wall thickness (mm)	4.0	1.25	Vertical 1.25, sloping 1	Vertical 1.25, sloping 1
Material	Aluminum	Aluminum	Aluminum	Aluminum
Material density (kg/m^3)	2800	2800	2800	2800
Young's modulus (Gpa)	3.3	3.3	3.3	3.3
Shear modulus (Gpa)	27.0	27.0	27.0	27.0
Natural frequency (rad/s)	714.0	198.1	154.1	370.2
Wave period (s)	1.85, 1.96, 2.08, 2.22	1.85, 1.96, 2.08, 2.22	1.85, 1.96, 2.08, 2.22	1.85, 1.96, 2.08, 2.22
Breaking wave height (m)	0.191~0.244	0.191~0.244	0.2~0.245	0.2~0.245
Water depth at the structures (m)	0.333	0.333	0.333	0.333

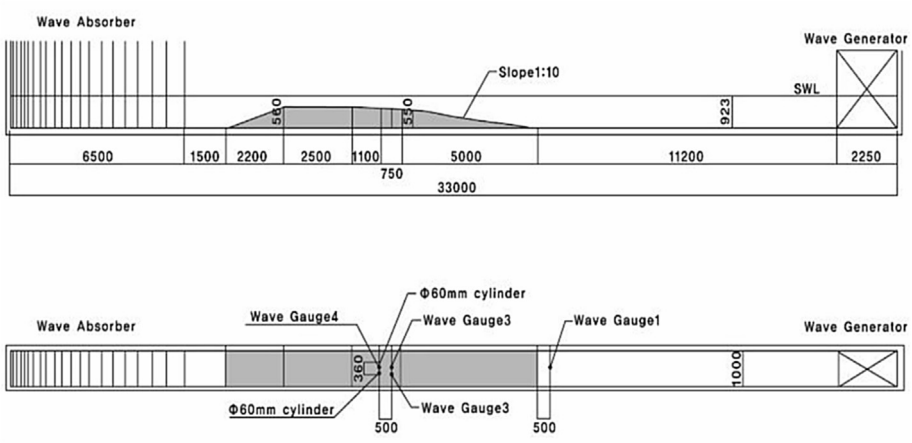

Fig. 5. Experimental flume (adapted from Navaratnam (2013)).

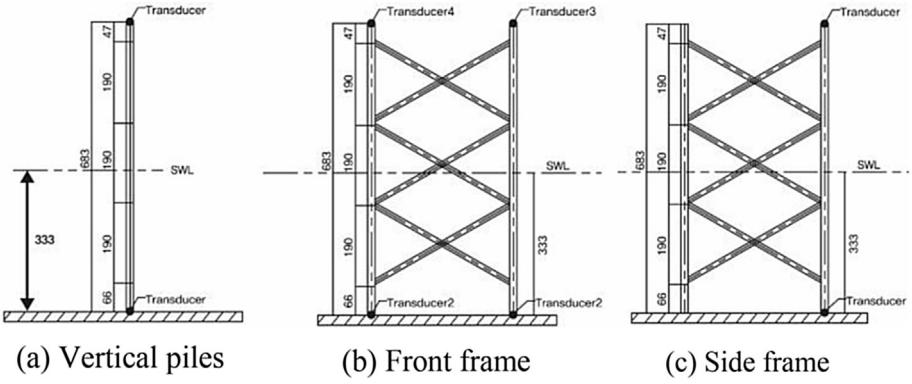

Fig. 6. Experimental structures and the locations of load cell meter (transducer).

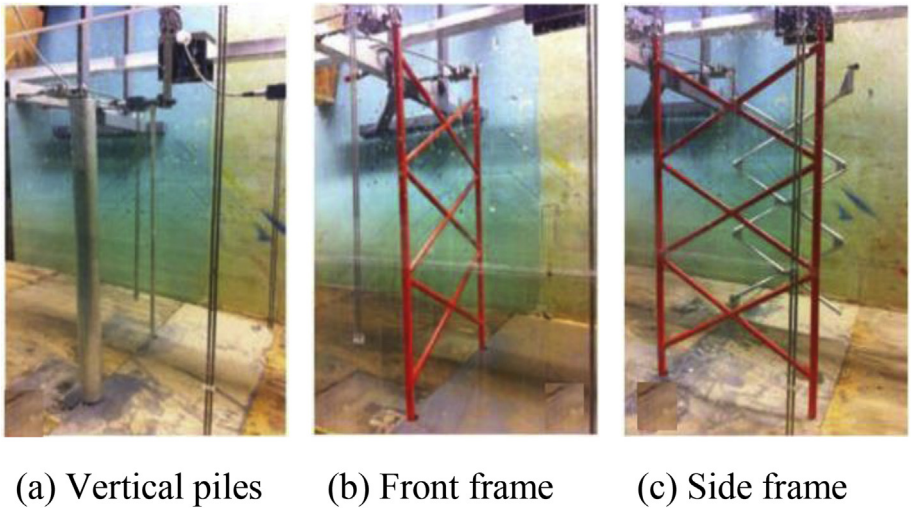

Fig. 7. Experimental structures placed inside the wave flume.

were transferred to the reaction forces. The slamming force was calculated by applying a transfer function to the reaction force signal. Navaratnam (2013) found this transfer function in advance using a hammer test that could relate the slamming force to reaction force. Fig. 8 shows the impingements of breaking waves on the Front and Side frames.

3.2. Dynamic analyses of experimental structures

Dynamic analyses were separately performed for all four cases listed in Table 2, and the results were compared with the experimental results. The hydrodynamic coefficients used in the analyses were taken as $C_D = 1.0$ and $C_I = 2.0$ which are

Fig. 8. Impingements of breaking waves to the experimental structures.

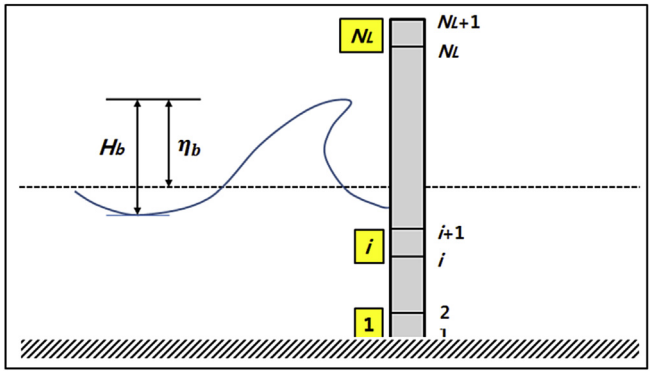

Fig. 9. Discretization of the piles into equal segments for the dynamic analysis.

generally accepted default values in the application of Morison's formula. The curling factor was chosen considering the range appeared in the existing researches (Goda et al., 1966; Wienke and Oumeraci, 2005), but the final value was taken as $\lambda = 0.4$ by tuning numerical results with the experimental results.

3.2.1. Cases 1 and 2

To verify the numerical analysis, the piles were divided into N_L equal segments, as shown in Fig. 9. The lumped areas and volumes of the joints between adjacent segments were calculated and input into the dynamic analysis. Joints 1 and $N_L + 1$ were constrained for all of the 6-DOF displacements by the attachment of the load cells in the experiment. Hence, the number of layers considered in the dynamic analysis was $N_L - 1$ from joint 2 to joint N_L. In the present verification work, the value of N_L was varied (5, 10, 15, or 20) to determine the effect of the number of layers on the calculation results.

The wave height H_b and wave crest height η_b in the dynamic analysis were considered to be the same as those of the experiment. Trial calculations showed that the duration of slamming force is in the range of 0.004–0.018 s for all lumped areas of the experimental structures. The time increment in the dynamic analysis was taken 0.0001 s which is very short enough to surely accommodate the slamming force durations and the natural frequencies in Table 2. The total number of calculation steps was 50,000.

The time variations of the total slamming reaction forces are shown in Fig. 10 for the experimental condition of case 1 at $T = 1.85$ s and $H_b = 0.234$ m. Here, the value of N_L was five. The total reaction forces were obtained by summing the reaction forces calculated at joints 1 and $N_L + 1$.

It can be seen from the figures that both slamming and reactions forces instantaneously occurred at the crests of the wave profile. The reaction force showed an oscillation corresponding to the natural frequency of the pile, as shown in

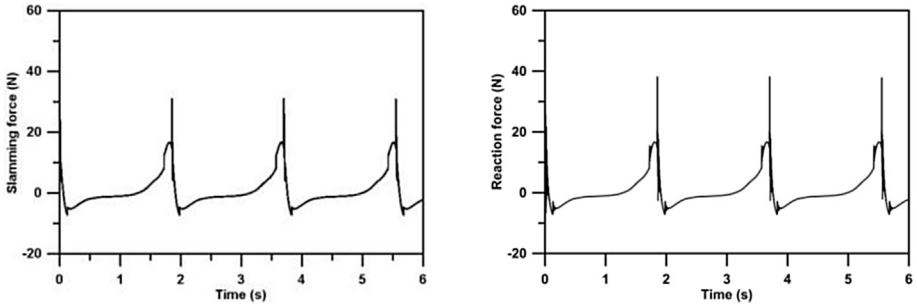

Fig. 10. Time variation of calculated total forces for Case 1 ($T = 1.85$ s and $H_b = 0.234$ m).

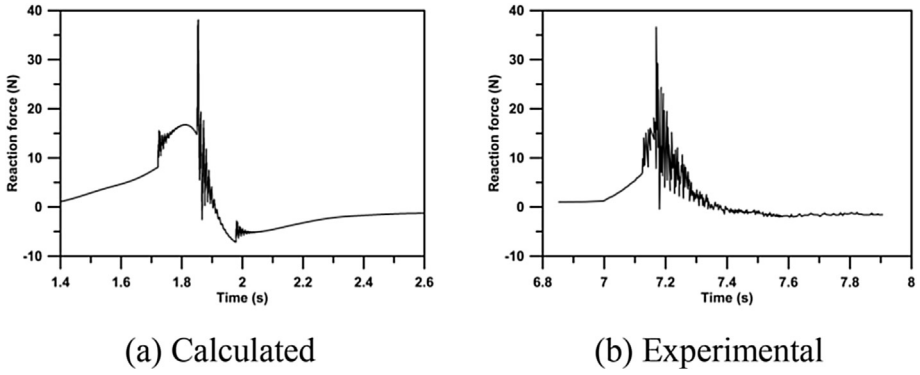

Fig. 11. Comparison of calculated and experimental reaction forces for Case 1 ($T = 1.85$ s and $H_b = 0.234$ m).

Fig. 11(a), which magnified a peak of Fig. 10(b). The duration of slamming force acting on the lumped area is about 0.02 s (see Eq. (24)). We can see that the oscillation continues far beyond the slamming force duration. This kind of oscillation was also well observed in the experimental results, as shown in Fig. 11(b).

3.2.2. Cases 3 and 4

The structures were comprised of 17 elements and 12 joints, and the numbering of the members and joints is shown in Fig. 12.

For the dynamic analysis, the number of layers for both structures was set at $N_L = 4$ (layers 2–8, 3–9, 4–10, and 5–11). In the numerical analysis, the joints where reaction forces were measured were all treated as fixed boundary conditions constraining all of the 6-DOF displacements (joints 1, 6, 7, and 12 in Case 3; Joints 1 and 6 in Case 4).

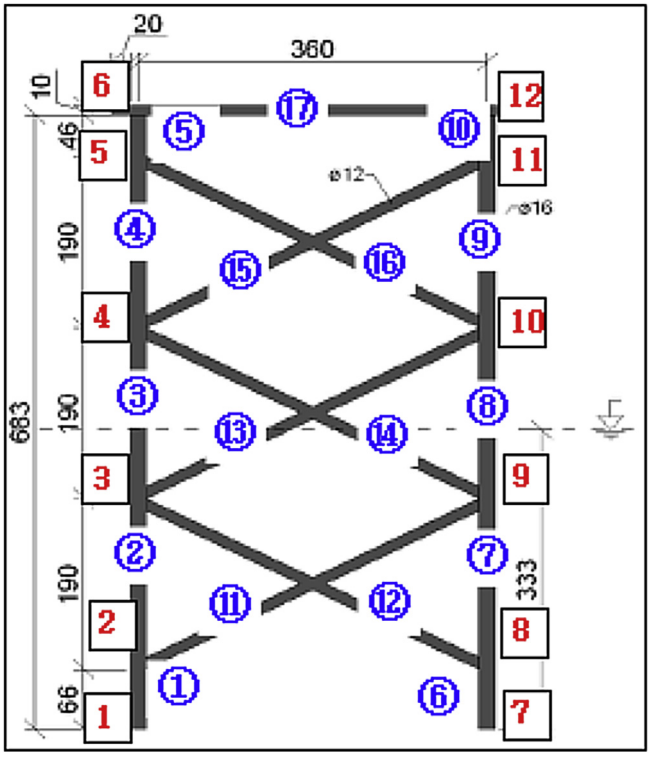

Fig. 12. Numbering of members and joints for the structures of Cases 3 and 4.

The total reaction force of the side frame for $T = 2.22$ s and $H_b = 0.231$ m is shown in Fig. 13(a). The oscillation of the structure at the impact of the breaking wave forces can also be seen in the experimental results of Fig. 13(b). The slamming force duration on the lumped areas in this case is about 0.0041 s.

4. Results and discussion

4.1. Cases 1 and 2 (monopiles)

The maximum slamming and reaction forces in the numerical analysis are selectively presented in Figs. 14–17, together with the corresponding experimental results. The numerical results show a monotonous increase with an increase in the breaking wave height, whereas the experimental results show quite a few scattered values. The dependency of the numerical results on the number of layers appeared to be very small, which indirectly supports the validity of the numerical algorithm in Table 1.

4.2. Case 3 (front) and case 4 (side)

Some selective numerical and experimental results are compared in Figs. 18–21. In both case 3 and case 4, the calculated slamming forces appeared to greatly exceed the experimental results, which was a contrast to cases 1 and 2. The discrepancies of slamming force can be partly due to the interference among structural members which was not taken into account in the present analysis. The slamming forces were calculated using Goda's formula (Eq. (21)). As previously mentioned, however, the slamming forces in the experiment were deduced from the measured reaction force using transfer functions, which were separately determined through hammer tests. The hammer tests were done in such a way that a hammer hit a specific point of the structure, with the reaction forces measured by a load cell embedded in the hammer. Depending on which point of the structure was hit by the hammer, the extracted transfer function could appear to be more or less different. The uncertainty of the hammer test may increase with an increase in the structural complexity. This may be why the slamming force discrepancies of cases 3 and 4 appeared to be greater than those of cases 1 and 2. Navaratnam (2013) also calculated much larger slamming forces than the

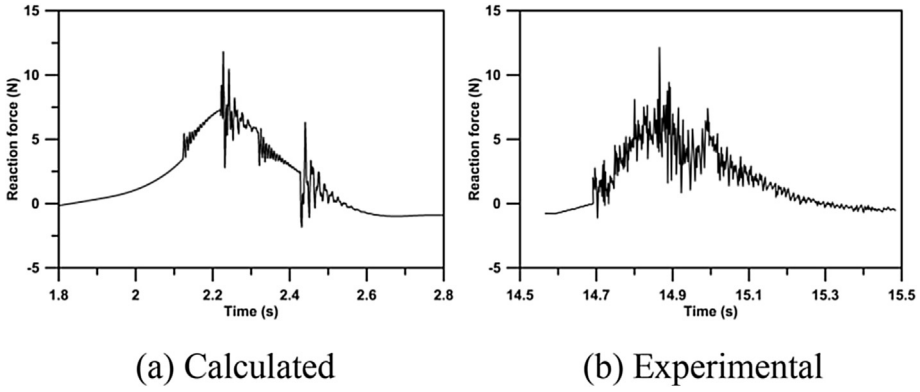

Fig. 13. Comparison of calculated and experimental reaction forces for Case 4 ($T = 2.22$ s and $H_b = 0.231$ m).

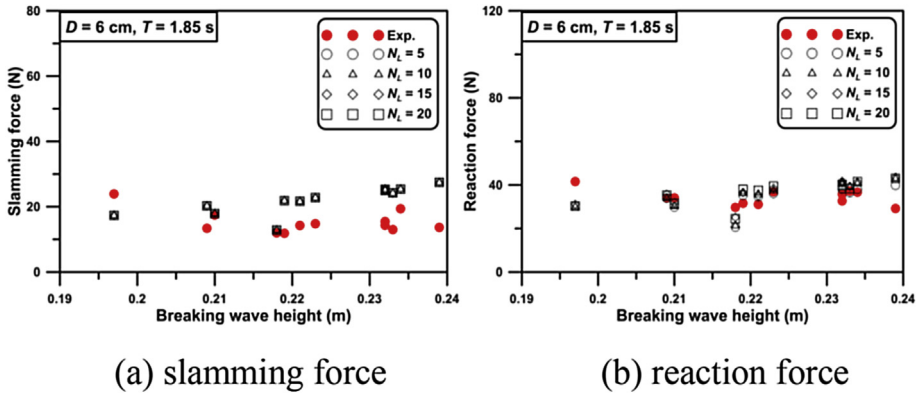

Fig. 14. Comparison of maximum slamming and reaction forces between numerical analyses and experiment (Case 1, $T = 1.85$ s).

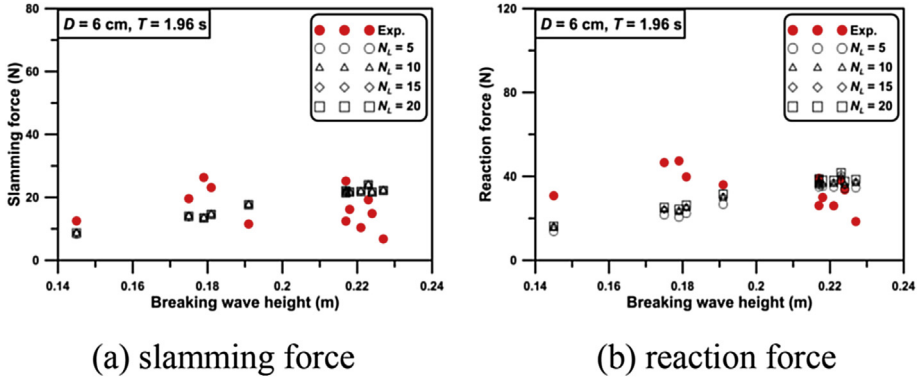

Fig. 15. Comparison of maximum slamming and reaction forces between numerical analyses and experiment (Case 1, $T = 1.96$ s).

experimental values. On the other hand, the reaction forces generally retained good agreement between the numerical and experimental results.

4.3. Analysis of relative error

For a more quantitative analysis of the accuracy of the numerical analysis, the relative error of Eq. (25) was calculated for all the experimental cases.

$$E = 1 - \frac{x_{\text{exp}}}{x_{\text{cal}}} \tag{25}$$

Here, x_{exp} and x_{cal} denote the experimental and calculated values, respectively. The mean values (E_s, E_r) and standard deviations (SD (E_s), SD (E_r)) of the standard errors covering all of the wave heights for each wave period are listed in Table 3, where the subscripts s and r denote the slamming force and reaction force, respectively. It is seen that E_s in cases 1 and 2 is distributed from 0.09 to 0.59, while E_r is within 0.3. In cases 3 and 4, however, E_s increases to 0.73–0.88, while E_r still remains within about 0.3. As previously mentioned, the slamming force bears an uncertainty related to the hammer test. Thus, focusing on the reaction force at least, it can be judged

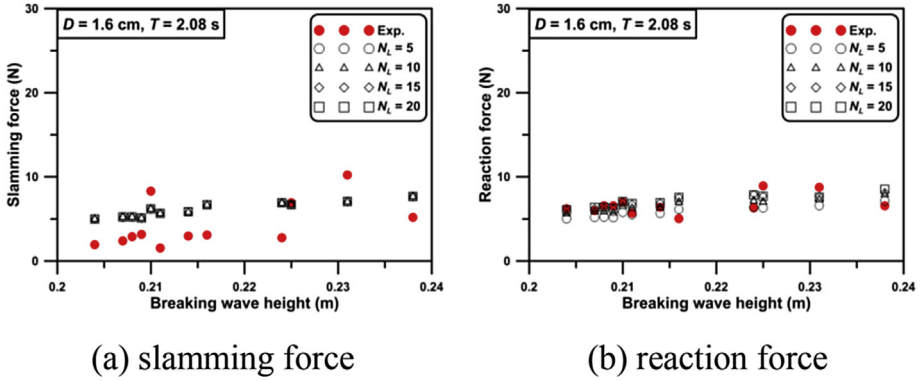

Fig. 16. Comparison of maximum slamming and reaction forces between numerical analyses and experiment (Case 2, $T = 2.08$ s).

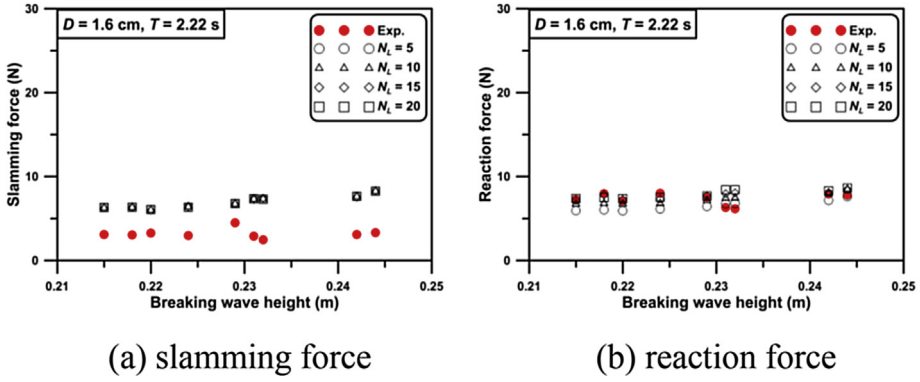

Fig. 17. Comparison of maximum slamming and reaction forces between numerical analyses and experiment (Case 2, $T = 2.22$ s).

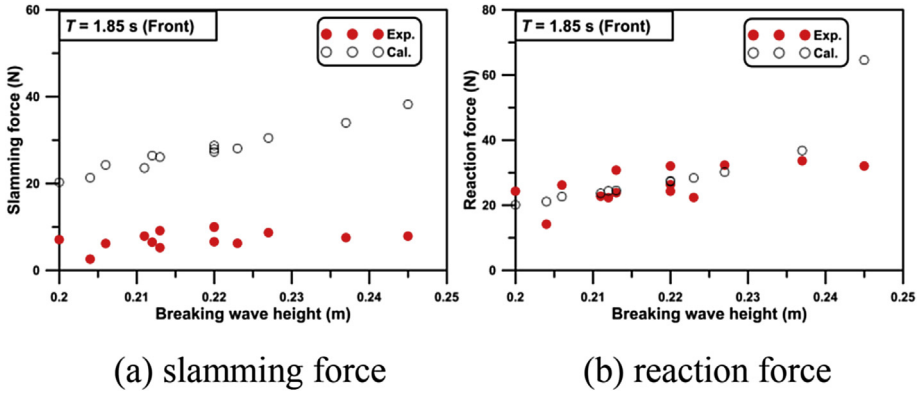

Fig. 18. Comparison of maximum slamming and reaction forces between numerical analyses and experiment (Case 3, $T = 1.85$ s).

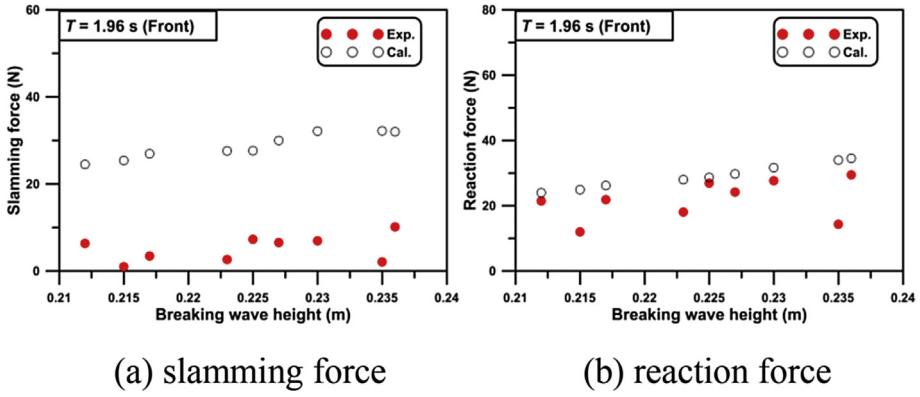

Fig. 19. Comparison of maximum slamming and reaction forces between numerical analyses and experiment (Case 3, $T = 1.96$ s).

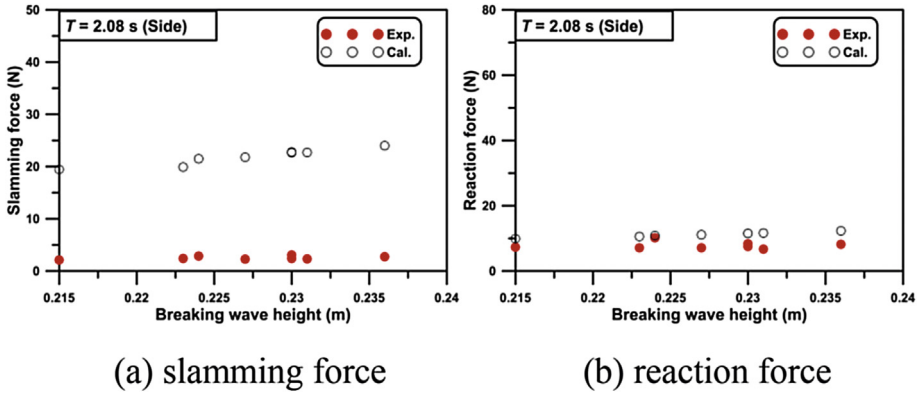

Fig. 20. Comparison of maximum slamming and reaction forces between numerical analyses and experiment (Case 4, $T = 2.08$ s).

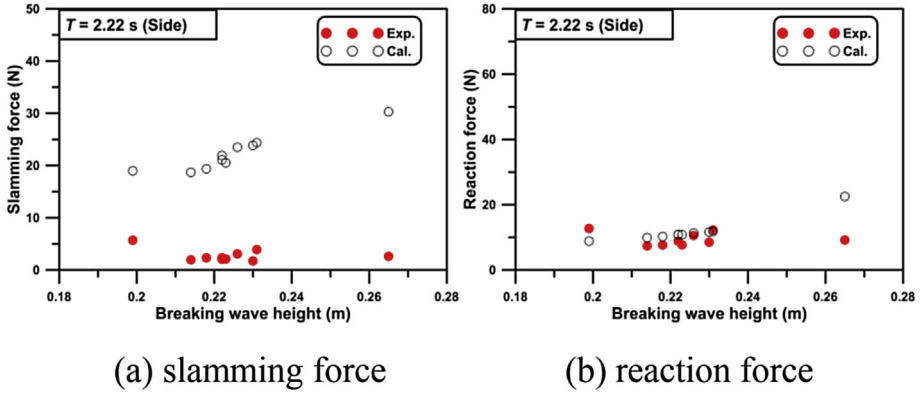

Fig. 21. Comparison of maximum slamming and reaction forces between numerical analyses and experiment (Case 4, $T = 2.22$ s).

that the numerical results generally agreed with the experimental results.

4.4. Discussion on experimental breaking waves

In the previous comparison of reaction forces, it was shown that the experimental results had somewhat scattered values, and even very peculiar outliers. This may have been due to the method used for generating breaking waves in the experiment. This method may have to be scrutinized to improve the quality of the comparison between the numerical and experimental results.

Most of the previous hydraulic experiments with breaking waves have used depth-induced breaking waves that were generated through wave shoaling on a sloped bottom inside a wave flume. The breaking wave depth and height on the slope were uniquely determined based on the input wave conditions of the wave period, height, and wave depth upstream of the flat bottom. Goda et al. (1966) used these kinds of breaking waves to extract Eq. (21), which has also provided the basis for the present numerical analysis. On the other hand, Wienke and Oumeraci (2005) generated breaking waves in their experiment by controlling the phase of the component parts of an irregular wave and concentrating them at a test point inside the wave flume. An experiment by Navaratnam (2013) generated breaking waves by making use of the inflection of bottom slopes.

When arbitrary waves inclining on a sloped bottom meet a flat or less-sloped bottom, the waves are easily broken even if the waves do not reach the depth-induced wave breaking depth on a provisionary continuous slope. Fig. 22 shows the breaking wave occurrence just downstream of the inflection point, which was reproduced by a CFD solver, CADMAS-SURF (CDIT,

Table 3
Relative error of the experimental values with respect to the calculated values.

Cases	T (s)	Structure	E_s	SD (E_s)	E_r	SD (E_r)
1	1.85	Pile (ϕ 60)	0.27	0.24	−0.02	0.20
	1.96	”	0.01	0.50	−0.31	0.61
	2.08	”	0.46	0.10	0.18	0.09
	2.22	”	0.25	0.26	0.06	0.25
2	1.85	Pile (ϕ 16)	0.06	0.59	−0.23	0.35
	1.96	”	0.26	0.29	−0.24	0.34
	2.08	”	0.32	0.37	−0.15	0.17
	2.22	”	0.54	0.09	−0.13	0.14
3	1.85	Front	0.73	0.07	0.04	0.20
	1.96	”	0.82	0.09	0.25	0.18
	2.08	”	0.69	0.10	−0.02	0.16
	2.22	”	0.74	0.07	0.06	0.20
4	1.85	Side	0.80	0.14	0.22	0.33
	1.96	”	0.85	0.04	0.20	0.23
	2.08	”	0.88	0.01	0.30	0.10
	2.22	”	0.87	0.06	0.16	0.25

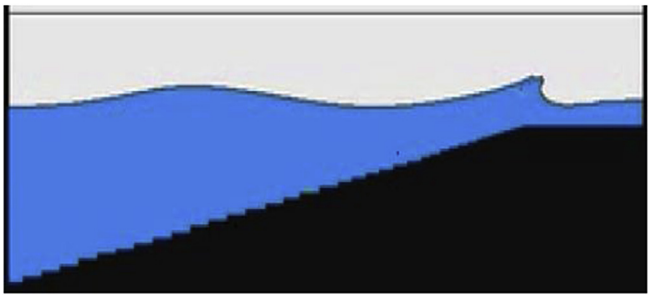

Fig. 22. CFD representation of breaking wave occurrence at the inflection point between a slope and downstream flat bottom.

2001). The waves likewise collapsed into breaking waves just downstream of the inflection point. The present experiment generated breaking waves using this kind of slope change from 1/10 to 1/20. The kinematic properties of these breaking waves may have been somewhat different from those of purely depth-induced breaking waves in that the breaking wave positions of all the input waves were fixed at the inflection point. The traveling distance of the breaking waves may have also been different, depending on the input wave conditions. These differences may have caused some uncertainties in the measured values of both the slamming and reaction forces.

The wave crest heights of the experimental breaking waves were also calculated using the 9th order stream function wave theory (Rienecker and Fenton, 1981) and compared with the measured crest height. Fig. 23 shows the variation of the relative crest height η_b/H_b versus H_b in both the calculated and experimental results. The calculated value of η_b/H_b slightly increases with an increase in H_b. However, the experimental values are mostly smaller than the calculated values, showing a fairly scattered pattern.

The experimental breaking waves were thus more or less different from the purely depth-induced breaking waves. This might have caused some deviations in the detailed kinematic structures of the breaking waves in the experiment compared to the purely depth-induced ones, producing the scattered patterns of the experimental results. The difference between the numerical and experimental results might be partly due to this discrepancy, even though the numerical analyses used experimentally measured breaking wave properties as their input conditions.

4.5. Recommendation for use of present numerical analysis

The following procedure is recommended for a prototype application of the present numerical analysis.

- Find the shallow water design wave condition by applying a nonlinear wave propagation model to the shallow water

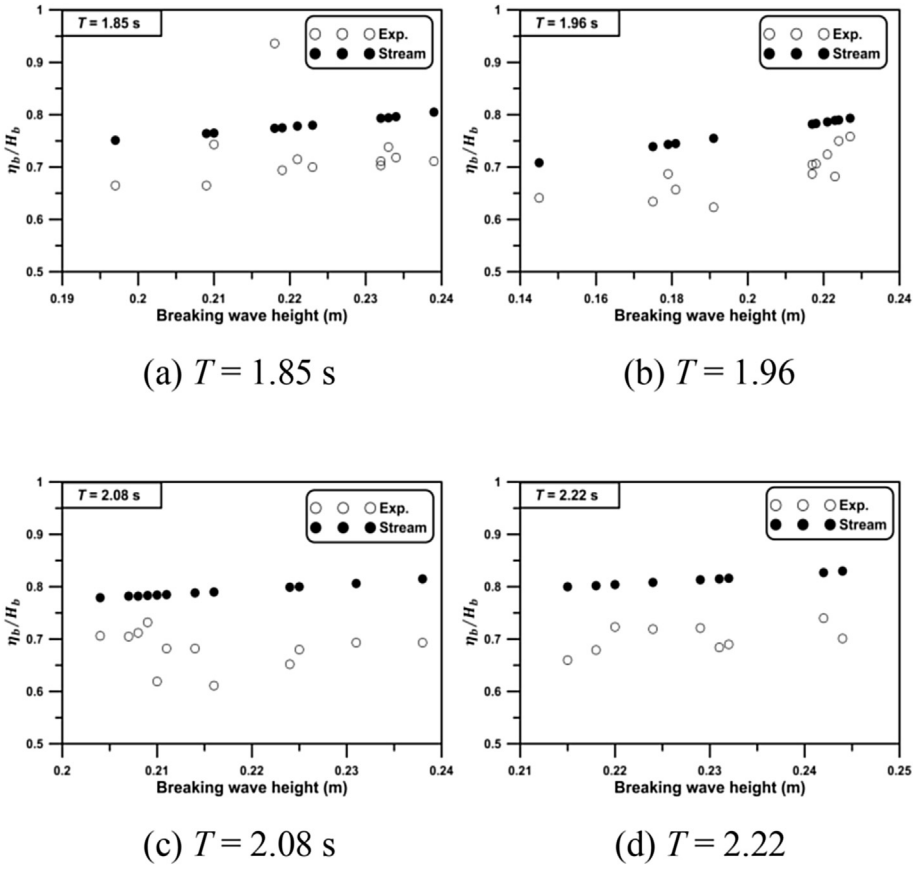

Fig. 23. Relative wave crest height versus breaking wave height.

zone where the prototype structure is placed. The input wave condition is either a deep sea design or stormy wave condition.
- Obtain the maximum wave and crest heights of the waves at the structure using the result of the wave propagation model. The result will automatically set the minimum deck clearance between the water surface and the lowermost deck. If necessary, adjust the deck levels.
- Investigate the possibility that the structure is captured by breaking waves. If captured, perform both static and dynamic analyses with the breaking wave condition (wave period, wave and crest heights).
- The structural response and member stresses are analyzed and compared with their allowable values. If necessary, adjust the dimensions of the structural members.

A demonstration of this procedure was presented by Woo (2015) and Chun et al. (2016) for a prototype jacket structure installed on an underwater shoal in Korea. The structure had been known to be frequently captured by breaking waves and was significantly damaged by typhoons in 2010 and 2011. Both horizontal displacement and member stresses calculated by the dynamic analysis with breaking wave were about 5–6 times larger than those by a static analysis with the regular wave condition having the same wave height and period.

5. Conclusion

The present study formulated a numerical method for performing dynamic analyses of 3D framed jacket structures subjected to arbitrary wave conditions. The dynamic analysis utilized a lumped mass method that calculates equivalent wave forces on each lumped mass pre-defined on the structure. The slamming forces on the lumped masses by breaking waves were calculated using an existing semi-empirical formula. The detailed results are as follows.

- An algorithm was devised to distribute the slamming force to pre-defined layers using the force–moment principle for a simple beam, which can be virtually postulated using two vertically adjacent layers. Each layer consisted of multiple lumped masses, which were defined differently depending on the structures concerned. The validity of the algorithm was tested using existing experimental results. The results showed that the effects of the number of layers on the dynamic responses are relatively negligible, which may justify the use of the algorithm in jacket structures that can be segmented into a few layers.
- A comparison was made of the slamming force and reaction force in the numerical and experimental results of monopiles. The reaction forces agreed with a 30% relative error based on the calculated values. In the framed structures, however, the slamming forces showed quite a few discrepancies. There may be numerous reasons for this, but the major reason could be attributed to the method for determining the slamming force in the hydraulic experiment. In the experiment, the slamming forces were indirectly obtained by applying a transfer function extracted from a separate hammer test to the experimentally measured reaction forces. This transfer function could be somewhat different depending on the position of the hammer impact compared to the experimental structures.
- In the numerical analysis, both the slamming and reaction forces tended to increase with an increase in the breaking wave height, but this tendency was not conspicuous in the experimental results. This may be attributed to the method of breaking-wave generation used in the experiment, where all the breaking waves were made just downstream of the inflection point of the bottom slope. These breaking waves could have been different from those generated on a monotonously sloped bottom in relation to the kinematic properties of the breaking waves. This might have produced the scattered pattern of experimental results, which finally caused the difference between the numerical and experimental results.

Finally, a recommended procedure for the application of the present numerical method to arbitrary 3D prototype structures was proposed.

Acknowledgements

The publication was supported by the Korea Institute of Ocean Science and Technology in relation to the project, “Construction of Ocean Research Station and their Application Studies” funded by the Ministry of Ocean and Fisheries, Korea in 2016.

References

Aashamar, M.Z., 2012. Wave Slamming Forces on Truss Support Structures for Wind Turbines. Master's thesis. Norwegian University of Science and Technology.

Apelt, C.J., Piorewicz, J., 1987. Laboratory studies of breaking wave forces acting on vertical cylinders in shallow water. Coast Eng. 11 (3), 263–282.

Bathe, K.J., 1982. Finite Element Procedures in Engineering Analysis. Prentice-Hall, pp. 508–511.

Brebbia, C.A., Walker, S., 1979. Dynamic Analysis of Offshore Structures. Newnes-Butterworths, pp. 256–257.

Campbell, I.M.C., Weynberg, P.A., 1980. Measurement of Parameters Affecting Slamming. Final Report, Rep. No. 440, Technology Reports Centre No. OT-R-8042, Southampton University: Wolfson Unit for Marine Technology.

CDIT, 2001. Research and Development of Numerical Wave Channel (CADMAS-SURF). Coastal Development Institute of Technology (in Japanese).

Chella, M.A., Tørum, A., Myrhaug, D., 2012. An overview of wave impact forces on offshore wind turbine substructures. Energy Procedia 20, 217–226.

Choi, S.-J., Lee, K.-H., Gudmestad, O.T., 2015. The effect of dynamic amplification due to a structure's vibration on breaking wave impact. Ocean. Eng. 96, 8–20.

Chun, I., Woo, C., Navaratnam, C.U., Shim, J., 2016. Design Wave Condition and Structural Analysis for Jacket Structures Installed in Wave Breaking Zone. Proc. of the 26th International Ocean and Polar Engineering Conference, Rhodes, Greece (to be published).

Dalton, C., Nash, J.M., 1976. Wave Slam on Horizontal Members of an Offshore Platform. Offshore Tech Conf, OTC-2500, Houston, TX, pp. 769–775.

Dawson, T.H., 1983. Offshore Structural Engineering. Prentice Hall.

Goda, Y., Haranaka, S., Kitahata, M., 1966. Study of impulsive breaking wave forces on piles. Rep. Port Harb. Res. Inst. 5 (6).

Greenhow, M., Li, Y., 1987. Added masses for circular cylinders near or penetrating fluid boundaries – review, extension and application to water-entry, -exit and slamming. Ocean. Eng. 14 (4), 325–348.

Hall, M.A., 1958. Laboratory Study of Breaking Wave Forces on Piles. TM-106, U.S. Army, Corps of Engineers, Beach Erosion Board, Washington, D.C.

Honda, T., Mitsuyasu, H., 1974. Experimental study of breaking wave force on a vertical circular cylinder. Coast Eng. Jpn. 17, 59–70.

Kjeldsen, S.P., Tørum, A., Dean, R.G., 1986. Wave Forces on Vertical Piles by 2- and 3-Dimensional Breaking Waves. Proc 20th Int Conf Coast Eng, Taipei, Taiwan, ASEC, pp. 1929–1942.

Navaratnam, C.U., 2013. Wave Slamming Forces on Truss Structures for Wind Turbines. Master's thesis. Norwegian University of Science and Technology.

Ross, C.W., 1959. Large-scale Tests of Wave Forces on Piling. TM-111, U.S. Army, Corpse of Engineers, Beach Erosion Board, Washington, D.C.

Rienecker, M.M., Fenton, J.D., 1981. A Fourier approximation method for steady water waves. J. Fluid Mech. 104, 119–137.

Sarpkaya, T., 1978. Wave Impact Loads on Cylinders. Offshore Tech Conf, OTC-3095, Houston, TX, pp. 169–176.

Tanimoto, K., Takahashi, S., Kaneko, T., Shiota, K., 1986. Impulsive Breaking Wave Forces on an Inclined Pile Exerted by Random Waves. Proc 20th Int Conf Coast Eng, Taipei, Taiwan, ASEC, pp. 2288–2302.

von Karman, T., 1929. The Impact of Sea Plane Floats during Landing. N.A.C.A. TN 321, Washington.

Wagner, H., 1932. Über Stoss und Gleitvongänge am der Oberfälche von Flüssigkeiten. ZAMM 12, 193–215.

Wiegel, R.L., 1982. Forces Induced by Breakers on Piles. Proc 18th Int Conf Coast Eng, Cape Town, South Africa, ASEC, pp. 1699–1715.

Wienke, J., Oumeraci, H., 2005. Breaking wave impact force on a vertical and inclined slender pile–theoretical and large-scale model investigations. Coast. Eng. 52 (5), 435–462.

Wilson, E.L., 2002. Three-dimensional Static and Dynamic Analysis of Structures. Computers and Structures, Inc., p. 19-6

Woo, C., 2015. Determination of the Shallow Water Design Wave and Structural Analysis for Jacket Structures Installed in Wave Breaking Zone. Doctoral dissertation. Dept. of Infra System Engineering, Konkuk University (in Korean).